Int. J. Heat Mass Transfer. Vol. 36, No. 16, pp. 3937–3947, 1993
Printed in Great Britain

0017–9310/93 $6.00+0.00

Unsteady behavior and mass transfer performance of the combined convective flow in a horizontal rectangular duct heated from below

H. KOIZUMI and I. HOSOKAWA
Department of Mechanical and Control Engineering, University of Electro-Communications, Chofu, Tokyo 182, Japan

(*Received* 10 *February* 1993 *and in final form* 28 *April* 1993)

Abstract—This paper reports a research for the mixed-convective flow and its mass transfer performance controlled by a preset side-wall temperature profile in a horizontal rectangular duct heated from below, which simulates a horizontal thermal Chemical Vapor Deposition (CVD) reactor. The experiment is carried out in a fully developed region at a Rayleigh number of about 3.4×10^5 to reveal various flow patterns depending on Reynolds number and the temperature profile on the side walls. Various unsteady flows are shown to be chaotic by calculating a set of Liapunov exponents from the observed time series of fluid temperature. In the case of an unsteady flow with time-averaged uniform temperature, the time-averaged mass transfer rate on the bottom wall of the duct becomes almost uniform in both the spanwise and the streamwise direction.

1. INTRODUCTION

HORIZONTAL thermal CVD reactors have been widely used for the process of producing thin layers of semiconductors, but a free convective effect to form stable longitudinal vortices in the process prevents the uniform growth of such layers. CVD reactors are operated with a combination of large Grashof number (Gr) and small Reynolds number (Re), that makes the value of $Gr/Re^2 = 10$–1000. For such flow systems a number of both numerical and experimental studies have been performed concerning the flow, temperature, deposition, and their development in the entrance regions [1–5].

Moffat and Jensen [1, 2] solved the steady-state, three-dimensional parabolized momentum, heat and mass-transfer equations with compressibility and variable physical properties to obtain the convective flow, temperature field and deposition performance in a horizontal rectangular duct. They revealed that the buoyancy-driven secondary flow had an undesirable effect on spatial uniformity of the growth rate and the flow structure is very sensitive to the thermal boundary condition on the walls of a reactor, the cross-section aspect ratio and the kind of carrier gas used. Van de Ven *et al.* [3] studied the growth rate of GaAs in the CVD process in a horizontal reactor with rectangular cross-section experimentally and theoretically. They showed that the growth rate was severely nonuniform in the lateral direction due to the natural convection occurring for a high Rayleigh number (Ra).

Furthermore, investigations of combined free and forced convection with application to CVD reactors revealed such a new flow behavior that the buoyancy-driven vortices can take many flow patterns including thermal instability of the flow for various combinations of Ra and Re. Chiu and Rosenberger [6] showed experimentally that the longitudinal rolls in combined convection between horizontal plates were unsteady like 'snaking'. Also, they showed the regime of the combination of Ra and Re leading to a steady or unsteady flow. Evans and Grief [5, 7] solved the two- and three-dimensional unsteady momentum and heat-transfer equations with compressibility to examine thermal instability in a horizontal duct. They showed that transverse, traveling waves can sweep periodically through a horizontal channel from inlet to outlet and such an instability greatly enhanced the average heat transfer rate.

These researches, which revealed the change of flow structure due to governing parameters such as Ra, Re and aspect ratio, are important both for operation of CVD reactors and for basic heat transfer science, but have hardly made a positive contribution towards the uniform growth of thin semiconductor layers so far. In this work, from the viewpoint that a properly preset side-wall temperature of the duct is an important factor for controlling the flow structure, we intend to destroy the stable rolls which prevent the uniform growth of a semiconductor layer by properly heating the side walls of the reactor. Our target of research is to find in what condition the buoyancy-driven longitudinal rolls can become so unsteady that the uniform growth may be attained. Then, all the change of flow characteristics by setting the side-wall temperature profile in various ways is investigated over a wide range of Reynolds number for a fixed Rayleigh number which is typical for CVD reactors. As a result, it is verified that the flow in the duct gets chaotic and,

NOMENCLATURE

a	horizontal width of duct
b	height of duct
D	coefficient of diffusivity
De	hydraulic diameter, $2ab/(a+b)$
d_m	embedding dimension
Gr	Grashof number, $g\beta(T_b-T_t)De^3/\nu^2$
h_D	local mass transfer rate
Pr	Prandtl number, ν/α
Ra	Rayleigh number, $Gr\,Pr$
Re	Reynolds number, $U_m De/\nu$
Sh	Sherwood number, $h_D De/D$
T	time-averaged temperature
t	fluctuating temperature
(U, V, W)	mean velocity components in x, y, z direction
(x, y, z)	rectangular coordinates, see Fig. 1(b)
x'	distance downstream from the leading edge of the aluminum tray where x' is set to zero.

Greek symbols

α	thermal diffusivity of fluid
β	coefficient of thermal expansion
δ	depth of naphthalene sublimation
$\Delta\tau$	sampling time
ε_r	radius of small ball
Θ	non-dimensional temperature, $(T-T_t)/(T_b-T_t)$
λ_L	Liapunov exponent
ν	kinetic viscosity of fluid
τ_{del}	delay time
τ_{dev}	evolution time.

Subscripts

b	bottom wall of duct
f	fluid
m	mean throughout the duct
swu	upper half of the side wall of duct
swl	lower half of the side wall of duct
t	top wall of duct.

at the same time, the time-averaged temperature distribution becomes horizontally uniform under certain suitable conditions. A naphthalene evaporation technique is employed to study the expectable mass transfer performance of the flows under these conditions. In order to elucidate the chaotic character of unsteady flows occurring for Reynolds numbers equal to and less than 220, we calculate a set of Liapunov exponents from the time series of fluid temperature. It is noteworthy that similar chaotic flows have recently been captured by a direct numerical simulation [8, 9] within the Boussinesq approximation and with the assumption that the flow is periodic in the longitudinal direction with a long period.

2. EXPERIMENTAL APPARATUS AND PROCEDURE

2.1. *Experimental apparatus*

Figure 1(a) shows a schematic view of the experimental apparatus, Fig. 1(b) the cross-section of the duct and the coordinate system, Fig. 1(c) the side-wall configuration, and Fig. 1(d) the aluminum tray which was used in the experiment of naphthalene sublimation. The cross section of the duct is rectangular, 30 mm in height and 60 mm in width. The top wall was made of copper plate and cooled by water. The bottom wall was made of 5 mm (Duct A) or 8 mm (Duct B) thick copper plate heated by a thin stainless steel foil, 10 μm thick, insulated from the copper plate. The foil was electrically heated. The top and bottom wall temperatures represented by T_t and T_b, respectively, are kept constant within 2% of the temperature difference between the two walls. In order to preset various profiles of the side-wall temperature, the side walls were divided in two halves and each of the halves were separately heated. For this purpose, two aluminum 30×30 mm^2 square ducts shown in Figs. 1(b) and (c) were used as side walls, on each of which two mica plates, 14 mm wide and 0.5 mm thick, were pasted; further, two independent thin stainless steel foils, 10 μm thick, were pasted on the mica plates to control the temperature of the side walls. Keeping the right-and-left symmetry, we produced various side-wall temperature profiles by adjusting both the amount of water flowing in the aluminum ducts and the amount of current through the steel foils. The temperature of the upper or lower half of each side wall was measured at the fully-developed flow section, as shown in Figs. 1(a) and (c) by three thermocouples of 0.1 mm diameter soldered on the back side of the steel foil with 3 mm intervals across the upper or lower half of the side wall and one thermocouple attached with tape at the center of the front surface of each foil. Then, the average of the temperatures measured by these four thermocouples indicates the upper temperature T_{swu} or lower temperature T_{swl} of each side wall. Two experimental apparatuses different in the full length of duct were used as indicated by A and B in Fig. 1(a). Duct A was used for measuring the temperature field [10], and Duct B for measuring the mass transfer rate by the naphthalene sublimation technique [11]. Duct A is 2300 mm in full length with a 5 mm thick copper bottom wall. The fluid temperature was measured at the section 1970 mm (49.3 De) downstream from the inlet and 330 mm (8.2 De) upstream from the outlet. Duct B is 1000 mm in full length with a 8 mm thick bottom wall, and the

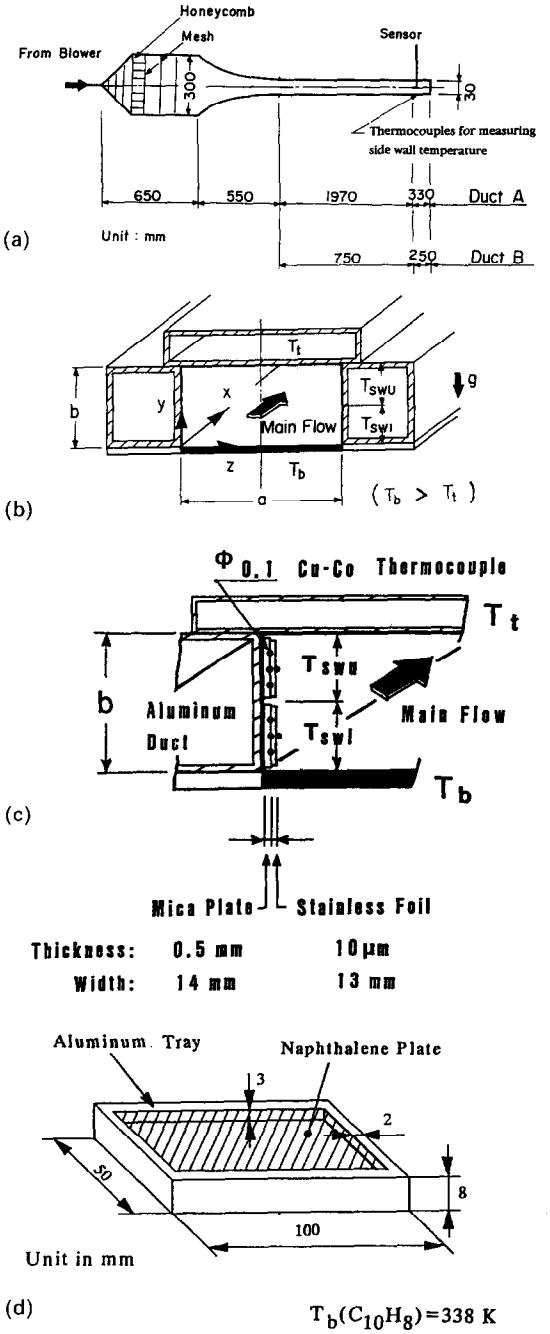

FIG. 1. Experimental apparatus. (a) Schematic view. (b) Cross-section of flow duct. (c) Side-wall configuration. (d) Aluminum tray.

naphthalene plate was set 750 mm (18.8 *De*) downstream from the inlet. The flows in these test sections were fully developed.

The working medium was air which was compressed by a blower and sent into the long horizontal rectangular duct downstream of a settling chamber, as shown in Fig. 1(a). The flow rate of air was measured by a float-area-type flow meter upstream of the settling chamber. The sensor of air temperature was a thermocouple of 50 μm diameter, which was equipped in the flow so as to have its sensing point 5 mm upstream of the supporting thin stainless L pipe of 1 mm outer diameter. This probe was inserted into the flow through the top wall at the fully-developed flow section, as shown in Fig. 1(a), and traversed in the cross section to measure a time-averaged temperature field T_f there. The experiment was performed mainly at a Rayleigh number of about 3.4×10^5 and for Reynolds numbers not greater than 500. The temperature of the side walls was changed in between those of the top and bottom walls. The Gr/Re^2 ratio, which is to govern the characteristics of a combined free and forced duct flow, was above 2 and therefore free convection was dominant.

2.2. *Analysis of fluctuating temperature*

The time-averaged temperature and temperature fluctuation intensity were obtained by calculating 30000 data sampled at 12 equi-spaced spanwise positions in the horizontal planes at $y/b = 0.25$, 0.50 and 0.75, using a microcomputer. Also, the power spectrum of temperature fluctuation was obtained by analyzing the output of the thermocouple of 50 μm diameter using an FFT analyzer. The response time of the thermocouple was about 0.13 s.

2.3. *Liapunov exponents*

The Liapunov exponents represent the time-development of the displacement vector between two very adjacent points in the phase space. The exponents can be calculated by the method proposed by Sano and Sawada [12], using the time series of fluid temperature observed at a certain point, as follows:

Using a time series $(T_f)_j = T_f(j\Delta\tau)$ $(j = 1, 2, \ldots, M)$, where M is the number of observations and $\Delta\tau$ is the time interval of sampling, an attractor can be reconstructed in a d_m-dimensional phase space by forming the vectors

$$(\vec{T}_f)_j = [(T_f)_j, (T_f)_{j+n}, \ldots, (T_f)_{j+(d_m-1)n}],$$

where $\tau_{del} = n\Delta\tau$ is the delay time, with the integer n chosen appropriately. In this study τ_{del} is chosen as the lag time at which the autocorrelation function of the time series falls to nearly zero.

Next, let us consider a small ball of radius ε_r centered at a particular orbital point $(\vec{T}_f)_j$, and find any set of N points $(\vec{T}_f)_{k_i}$ included in this ball to make the displacement vector $\vec{\zeta}^i = (\vec{T}_f)_{k_i} - (\vec{T}_f)_j$ $(i = 1, \ldots, N)$. After time interval τ_{dev}, the $\vec{\zeta}^i$ will evolve to $\vec{\xi}^i$ as shown in Fig. 2. If ε_r is small enough, the dynamical development may be linearly approximated by a matrix, $A(\tau_{dev})$, as

$$\vec{\xi}^i = A(\tau_{dev})\vec{\zeta}^i.$$

$A(\tau_{dev})$ is approximately obtained by using the displacement vectors $\vec{\zeta}^i$ and $\vec{\xi}^i$ [12]. Then, the Liapunov exponent λ_L can be computed as

$$\lambda_L = \langle (1/\tau_{dev})[\ln \| A(\tau_{dev})\hat{e}_L \|] \rangle \quad (L = 1, \ldots, d_m)$$

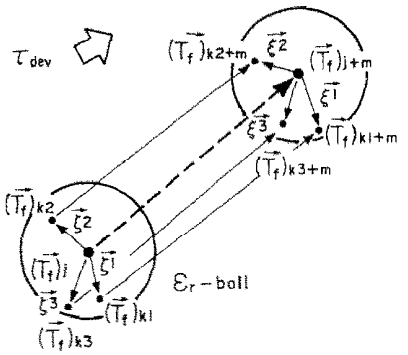

FIG. 2. Orbits of points in time evolution τ_{dev} in the d_m-dimensional phase space.

where $\langle \ldots \rangle$ is the ensemble average over similar developments of many successive phase points along the trajectory of $(\vec{T}_f)_j$, $\vec{e}_L$ is the eigen vector of unit length, and $\| \ldots \|$ indicates the norm of a vector.

A set of Liapunov exponents arranged in decreasing order is called a Liapunov spectrum. When one or more positive exponents are obtained, the flow may be characterized as chaotic with the magnitude of the exponents indicating the time scale for predictability.

The program in this study was tested on the x-component of the well-known Lorenz model with parameters $R = 40$, $\sigma = 16$, $b = 4$ [12, 13]. The integration was performed using the fourth-order Runge–Kutta method by taking the time step as 0.01, the delay time τ_{del} as 0.13 which is the same as that of Sano and Sawada [12], the radius of small ball as $0.015 \leqslant \varepsilon_r/L \leqslant 0.03$ (L is the horizontal extent of the attractor), the number of points N contained within the small ball as $d_m \leqslant N \leqslant 10$ and the evolution time as $0.05 \leqslant \tau_{dev} \leqslant 0.1$. The error bars were calculated from several runs with different parameters ε_r, N, τ_{dev} within the above mentioned ranges of values. A reasonable Liapunov spectrum of the Lorenz model was found from 65 536 data points by the present program. In the case of three-dimensional phase space, the results are shown in Table 1 and compared with the result of the time-delay method by Sano and Sawada [12] and the numerical result of Shimada and Nagashima [13]. In this case, our positive and zero exponents λ_1, λ_2 are in good agreement with these results [12, 13].

In analyzing the observed time series of fluid temperature including 65 536 data points, the developing time was $5\Delta\tau \leqslant \tau_{dev} \leqslant 10\Delta\tau$ for time step $\Delta\tau = 0.007812$ s. Typically, τ_{del} was about 0.7 s. When the extent of the phase space was normalized as unity, the radius of a small ball was $0.03 \leqslant \varepsilon_r \leqslant 0.05$, and the number of the phase points included in it was $10 \leqslant N \leqslant 20$. A tungsten cold wire of 5 μm diameter was used as a sensor of air temperature in this experiment.

2.4. *Mass transfer rate on the bottom wall*

We examined the mass transfer rate on the bottom wall in both cases of steady and unsteady flows using the naphthalene sublimation technique, which treats the inverse phenomenon to deposition in a thermal CVD reactor. The mass transfer experiment was performed in the fully developed region in Duct B. A naphthalene plate, 3 mm thick, 44 mm wide and 94 mm long, was pasted in the aluminum tray shown in Fig. 1(d) using double-sided tape, and this tray was embedded on the bottom wall made of 8 mm thick copper 750 mm downstream from the inlet. The tray was heated by two heaters independently, and the naphthalene surface temperature was kept constant at 338 ± 1 K. In order to protect deformation of the naphthalene plate, the naphthalene surface temperature was kept 10 K lower than that of the bottom wall. The shapes of the naphthalene surface, before and after the surface was exposed in the air flow for 40 min, were measured by a surface-shape measuring machine to give an amount of sublimation distribution $\delta(x, z)$. Using the δ and the sublimation time, we calculated the local time-averaged Sherwood number distribution [14]. The accuracy of this technique was checked on the laminar boundary layer flow along an unheated flat plate, somewhat behind the leading edge at which the sublimation occurs, and we confirmed that the experimental Sherwood number distribution was in good agreement with the theoretical one [15] within 3%.

3. EXPERIMENTAL RESULTS AND DISCUSSIONS

3.1. *Relation between the side-wall temperature profile and flow pattern*

The experiment revealed that at Reynolds numbers ranging from 140 to 500, steady or unsteady longi-

Table 1. Liapunov spectrum estimated for the Lorenz model

	Embedding This result	Embedding Sano and Sawada [12]	Numerical calculation Shimada and Nagashima [13]
λ_1	1.37 ± 0.15	1.37 ± 0.08	1.37
λ_2	0.0 ± 0.1	-0.02 ± 0.09	0.00
λ_3	-15 ± 4	-15.2 ± 2.1	-22.37

tudinal rolls were always observed, while at Reynolds number 140 or below, no specific vortices appeared and the flow was unsteady with a relative temperature fluctuation intensity of about 5–7%. Then, we present the results mainly at three Reynolds numbers which showed different flow patterns. Figure 3 shows the relations between the side-wall temperature profile and flow pattern for $Re = 500$, 220 and 90 [10, 11, 16–18]. A certain vortical structure in the flow may be judged to exist from the time-averaged fluid temperature distributions for various side-wall temperature profiles as shown in Fig. 4. Taking the non-dimensional upper-half side-wall temperature Θ_{swu} in ordinate and the lower-half side-wall temperature Θ_{swl} in abscissa, we classify the experimental results for $Re = 500$ in Fig. 3(a), for $Re = 220$ in Fig. 3(b) and for $Re = 90$ in Fig. 3(c). White marks in Fig. 3 show the data obtained by this experiment using Duct A in Fig. 1(a) and black ones those obtained by the previous work [16].

For $Re = 500$, there are two distinct regions in the $(\Theta_{swu}, \Theta_{swl})$ plane as is seen in Fig. 3(a). One is a spacious region II with a pair of vortices with upward flow along the side walls, shown by mark △, and the other is region IV with a pair of vortices with downward flow along the side walls, shown by mark ▽. Then it is clear that the vortical structure is changed by changing the side-wall temperature profile, the time-averaged fluid temperature distribution is never horizontally uniform, and two stable symmetric longitudinal rolls are always generated.

For $Re = 220$, new regions I and III with almost steady and unsteady flow, respectively, appear as is seen in Fig. 3(b). In regions I and II we have a pair of vortices with upward flow along the side walls, shown by mark △ and ▲. In region I, the relative temperature fluctuation intensity ($\sqrt{(t^2)}/T_f$; $\sqrt{(t^2)}$ is the root mean square of temperature fluctuation, and T_f is the local time-averaged fluid temperature) is below 0.6% and the horizontal fluid temperature distribution agrees with the numerical results obtained by solving the steady momentum and heat-transfer equations with the Boussinesq approximation [16–18]. However, in region II, the relative temperature fluctuation intensity is about 1–2.5% and the steady-state approach described above fails to yield a solution. In region III, shown by mark ◇ and ◆, even though two pairs of vortices were observed, they changed both their shape and position with time mainly horizontally, and the time-averaged temperature distribution in a horizontal plane was observed to be fairly flat. The relative temperature fluctuation intensity in this case is about 3% and almost uniform in the horizontal direction. In region IV, shown by mark ▽ and ▼, a pair of vortices appeared with downward flow along the side walls, which rotate in the direction opposite to that in region I. The relative temperature fluctuation intensity is about 1%.

For $Re = 90$, as is seen in Fig. 3(c), unsteady flows

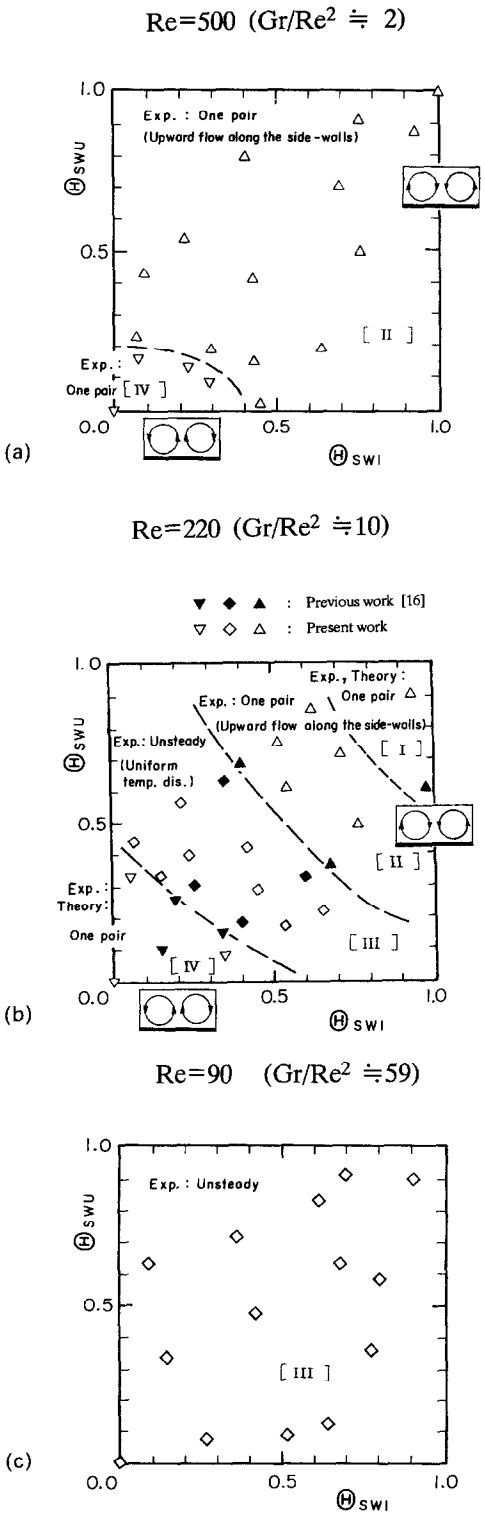

FIG. 3. Relation between the side-wall temperature and flow pattern for Reynolds number (a) 500 ($Gr/Re^2 \doteqdot 2$), (b) 220 ($Gr/Re^2 \doteqdot 10$) and (c) 90 ($Gr/Re^2 \doteqdot 59$), respectively.

are always produced for all side-wall temperature profiles, but the time-averaged fluid temperatures do not have a very flat distribution in the spanwise direction, especially near the bottom wall. The relative fluc-

tuating temperature intensity is about 5% for $Re = 90$ and increases with Reynolds number decreasing. When $Re = 0$, there occurs only a free convection and the same unsteady flow as shown in Fig. 3(c) is produced for all side-wall temperature profiles.

From the above-described results for Reynolds numbers not greater than 500, it is clear that the flow pattern is controlled by changing Reynolds number and the side-wall temperature profile, and the unsteady flow with time-averaged horizontally uniform temperature distribution can be produced by a proper adjustment of condition.

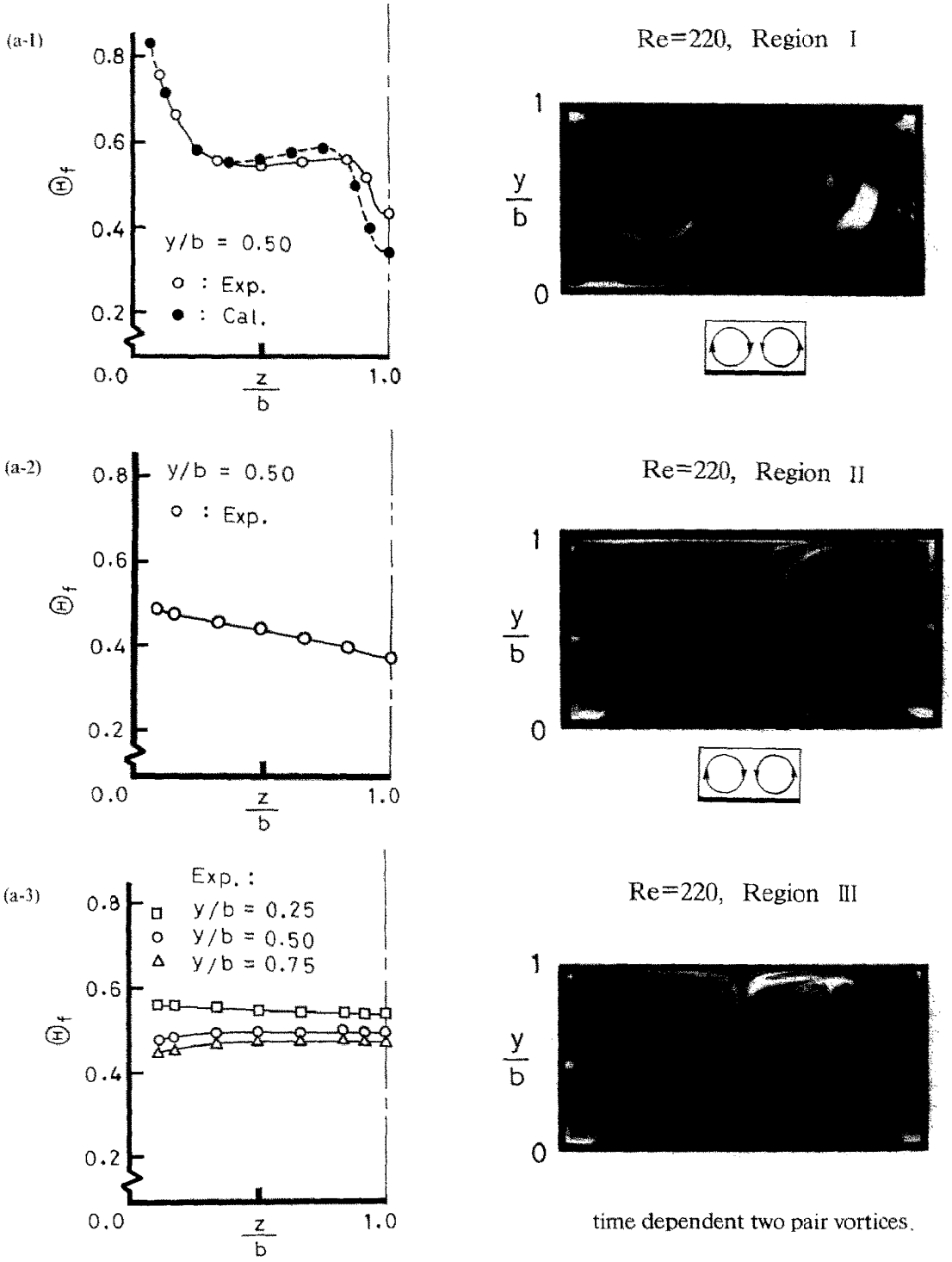

FIG. 4. Time-averaged temperature distribution and photo instantaneous flow visualization. (a-1) $Re = 220$ ($\Theta_{swu} = 0.60$, $\Theta_{swl} = 1.00$ in region I); (a-2) $Re = 220$ ($\Theta_{swu} = 0.56$, $\Theta_{swl} = 0.61$ in region II); (a-3) $Re = 220$ ($\Theta_{swu} = 0.33$, $\Theta_{swl} = 0.59$ in region III); (a-4) $Re = 220$ ($\Theta_{swu} = 0.10$, $\Theta_{swl} = 0.16$ in region IV); (b) $Re = 90$ ($\Theta_{swu} = 0.00$, $\Theta_{swl} = 0.00$ in region III).

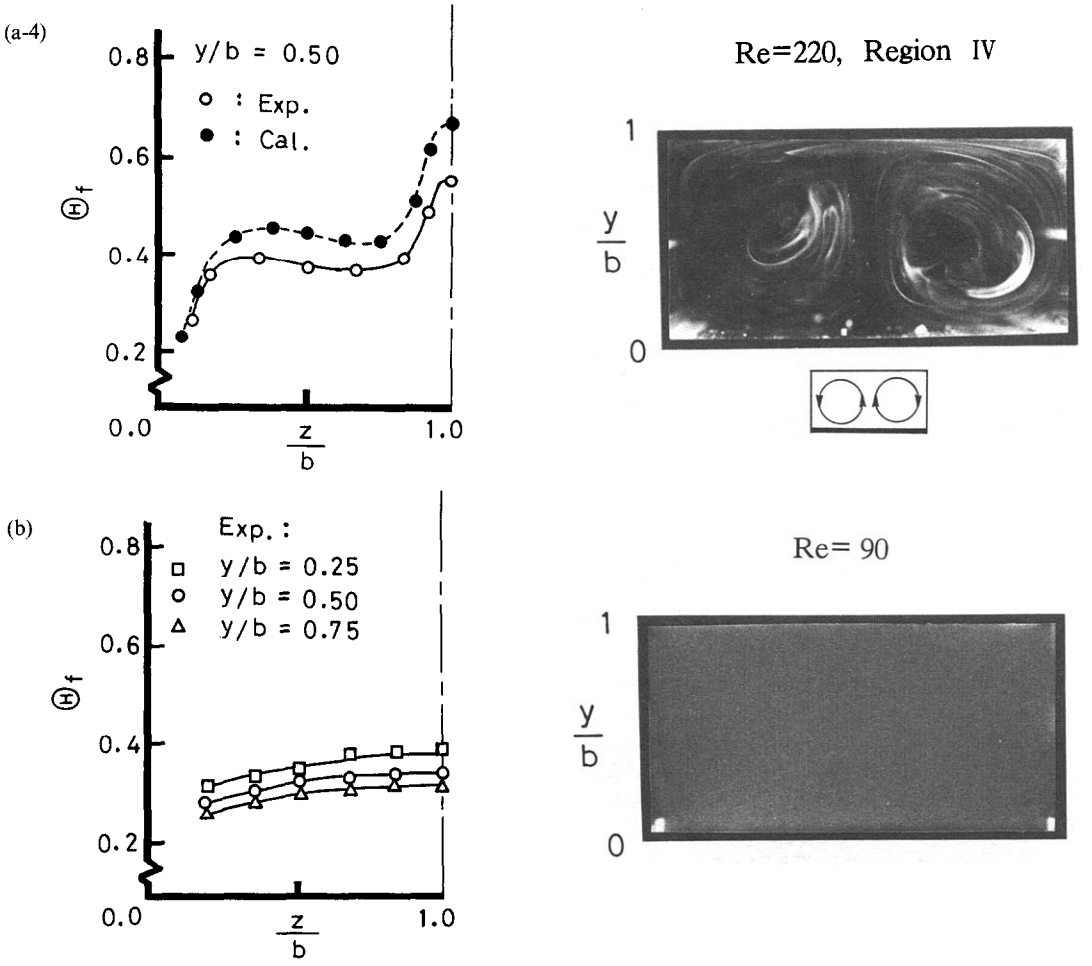

FIG. 4—*Continued.*

In order to investigate the Rayleigh number dependence of generation of an unsteady flow for a given Reynolds number such as $Re = 220$, we performed the experiment at a Rayleigh number of about 1.7×10^5 and $Re = 220$. The result shows that the decrease of Rayleigh number results in a slight upward movement of the unsteady flow region on the map of Fig. 3(b), so that the unsteady flow region is little influenced by the change of Rayleigh number of this degree.

We also performed the experiment at a Rayleigh number of about 3.4×10^5 for Reynolds number ranging from 2400 to 12000, which is in the fully-developed turbulent region. In this case, the time-averaged horizontal temperature distributions and the time-averaged flow patterns could change depending on Reynolds number and the side-wall temperature profile [19], but the longitudinal rolls observed by time-averaging was so stationary that no horizontally uniform temperature was achieved by any means.

3.2. *Time-averaged fluid temperature distribution and flow visualization*

Figure 4 shows the non-dimensional time-averaged fluid temperature distributions in a half cross-section of the duct and the corresponding instantaneous flow visualization photos for $Re = 220$ and 90.

For $Re = 220$ and in region I, the temperature distribution in a horizontal plane at the middle height of the duct is shown in Fig. 4(a-1). White circles indicate experimental points, and black ones the numerical results mentioned before [16–18]. The temperature is high near the side walls and low in the middle of the duct, so that it is considered that a pair of vortices with upward flow along the side walls have been produced in the duct. This is justified by a good agreement between the experiment and the numerical result. This flow pattern is also confirmed by the instantaneous flow visualization photo shown in Fig. 4(a-1). For $Re = 220$ and in region II, the experimentally observed temperature at the middle height of the duct shown in Fig. 4(a-2) by mark ○ is high near the side walls and is low in the middle, but any corresponding convergent numerical solutions were not found in this region [16]. This means that the flow can no longer be exactly steady. This flow pattern, more or less with a pair of vortices, is also confirmed by the photo shown in Fig. 4(a-2), but the circulation is not so clear as that of region I shown in Fig. 4(a-1), probably because of strong fluctuation. For $Re = 220$ and in

region III, the time-averaged experimental temperature distributions are shown in Fig. 4(a-3) by mark □ at $y/b = 0.25$, ○ at $y/b = 0.50$ and △ at $y/b = 0.75$, respectively. The three distributions are fairly uniform in each horizontal plane. From the photo shown in Fig. 4(a-3), two pairs of longitudinal vortices were observed to unsteadily move and change their shape with time. For $Re = 220$ and in region IV, the temperature distributions in a horizontal plane at the middle height of the duct are shown in Fig. 4(a-4). White circles are experimental points, while black circles are the numerical results [16–18]. The temperature is low near the side walls and high in the middle part, so that a pair of vortices with downward flow along the side walls have been produced. But the agreement of both experimental and numerical results is not so good as in region I of Fig. 4(a-1). This is also understood to be due to the nonlinear flow instability (as detected in the power spectrum to be described in Section 3.3) and then this flow is not really steady.

For $Re = 90$, the flow becomes very unsteady and Fig. 4(b) shows the time-averaged experimental temperature distributions at three horizontal planes. The three distributions are not very flat. From the photo shown in Fig. 4(b), no specific vortices can be seen. Therefore, for Reynolds numbers below 140 ($Gr/Re^2 > 24$) in this experiment, it may be reasonable to consider that the transverse rolls were generated in addition to the longitudinal rolls and made the flow unsteady regardless of the side-wall temperature profile, in the same way as Chiu and Rosenberger [6] suggested.

3.3. *Power spectra of temperature fluctuation*

In order to understand the temperature fluctuation in more detail, the power spectrum of fluid temperature was studied. Figure 5 shows the power spectrum measured by a thermocouple of 50 μm diameter at the position of $y/b = 0.5$ and $z/b = 0.3$. The results are shown for $Re = 500$ in Figs. 5(a-1) and (a-2), for $Re = 220$ in Figs. 5(b-1)–(b-4) and for $Re = 90$ in Fig. 5(c), respectively.

For $Re = 500$ and in region II, the spectrum has many peak frequencies as shown in Fig. 5(a-1), but the spacing of each peak does not show any specific rule. But in region IV, the spectrum in Fig. 5(a-2) has many peak frequencies, which are broadened but expressed as linear combinations of two basic frequencies, $f_1 = 0.05625$ Hz and $f_2 = 0.02500$ Hz. This indicates that the time-dependent process in this unsteady flow is strongly nonlinear and no less than quasi-periodic.

For $Re = 220$ and in region I, the relative temperature fluctuation intensity is less than 0.6% and the spectrum in Fig. 5(b-1) does not have any characteristic frequency, showing an almost steady state. In region II, the intensity is about 1–2.5% and the spectrum in Fig. 5(b-2) has many peak frequencies, but the spacing of each peak does not show any specific rule. In region III, the spectrum in Fig. 5(b-3) has many peak frequencies, broadened but expressed as linear combinations of two basic frequencies, $f_1 = 0.13750$ Hz and $f_2 = 0.01875$ Hz. The intensity is about 3% and almost uniform in the horizontal direction. In region IV, the spectrum in Fig. 5(b-4) is about the same except for $f_1 = 0.05625$ Hz and $f_2 = 0.02500$ Hz. The intensity is about 1%.

For $Re = 90$, the spectrum in Fig. 5(c) has similarly two basic frequencies, $f_1 = 0.08750$ Hz and $f_2 = 0.03125$ Hz. The intensity is about 5% and almost uniform in the spanwise direction.

From the above investigation, it is natural to think that some of these unsteady flows may be chaotic. This can be made sure by looking at the Liapunov spectra from the time series of fluid temperature in such flows.

3.4. *Evidence of chaotic flows*

The Liapunov spectrum was calculated from the temperature time-series at the position of $y/b = 0.5$ and $z/b = 0.3$. Some representative Liapunov spectra are shown in Table 2.

For $Re = 220$ and in region I, the Liapunov spectrum is $[3 \pm 2, -5 \pm 2, -20 \pm 7]$ for $d_m = 3$ and $[3 \pm 2, -3 \pm 2, -9 \pm 3, -28 \pm 7]$ for $d_m = 4$. In this flow the fluctuation intensity is below 0.6% and only a slight positive exponent appears. Then, we may judge that this flow is hardly chaotic. On the contrary, in the case of an unsteady flow for $Re = 220$ and in region III, we have $[21 \pm 5, 9 \pm 3, -13 \pm 8]$ for $d_m = 3$ and $[20 \pm 5, 12 \pm 4, -4 \pm 5, -18 \pm 8]$ for $d_m = 4$. Two positive exponents appear here, so that this flow is considered as strongly chaotic. For $Re = 90$ of an unsteady flow with the fluctuation of about 5%, we have $[11 \pm 3, 3 \pm 2, -11 \pm 7]$ and $[10 \pm 3, 3 \pm 2, -4 \pm 3, -17 \pm 7]$. This flow is also considered as chaotic.

Although the unsteady flows for $Re = 220$ in region III and for $Re = 90$ are both chaotic, their flow features seem to be considerably different from each other, as was discussed in Section 3.2. It would be instructive in future to clarify the meaning of the difference between the magnitudes of the maximum Liapunov exponents in both cases by a more precise method, such as a direct numerical simulation in which the evolutional Fourier spectrograph of the entire flow field is fully used for observing a chaos with many degrees of freedom [8, 9].

3.5. *Mass transfer performance on the bottom wall*

Figure 6 shows the local time-averaged Sherwood number distributions on the bottom wall for $Re = 220$ in both cases of steady and unsteady flows. The spanwise distributions at the central part of naphthalene (50 mm downstream from the leading edge of the aluminum tray) are shown in Fig. 6(a) and the streamwise distributions along the center line of the duct are in Fig. 6(b). In Fig. 6, marks ▽ and ◇ indicate the results for the side-wall temperature conditions of $\Theta_{swu} = \Theta_{swl} = 0.00$ and $\Theta_{swu} = 0.31$, $\Theta_{swl} = 0.15$, respectively. Figure 6(a) shows that in the former case,

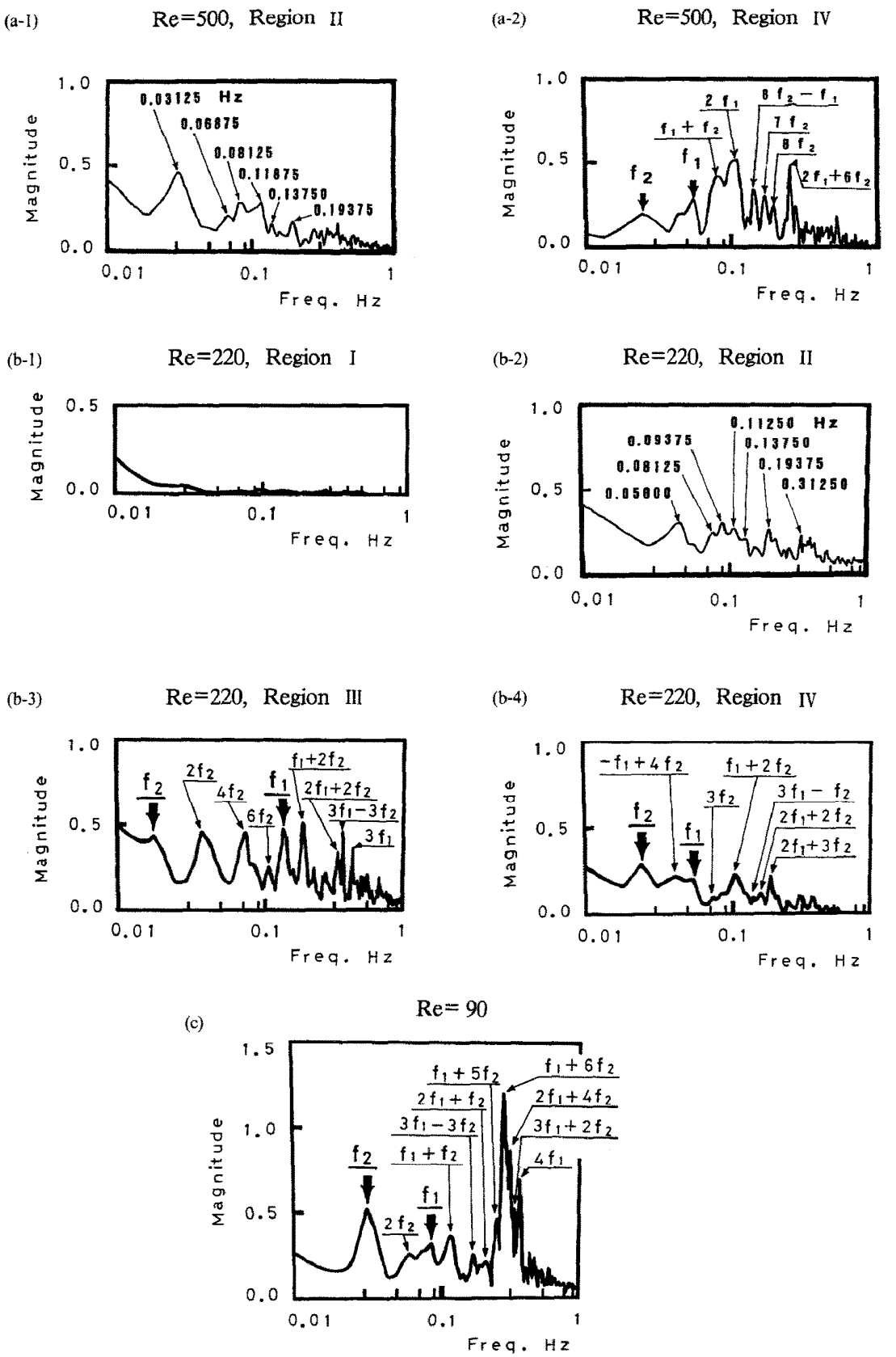

FIG. 5. Power spectrum. (a-1) $Re = 500$ ($\Theta_{swu} = 0.88$, $\Theta_{swl} = 0.93$ in region II); (a-2) $Re = 500$ ($\Theta_{swu} = 0.00$, $\Theta_{swl} = 0.00$ in region IV); (b-1) $Re = 220$ ($\Theta_{swu} = 0.90$, $\Theta_{swl} = 0.93$ in region I); (b-2) $Re = 220$ ($\Theta_{swu} = 0.56$, $\Theta_{swl} = 0.61$ in region II); (b-3) $Re = 220$ ($\Theta_{swu} = 0.22$, $\Theta_{swl} = 0.67$ in region III); (b-4) $Re = 220$ ($\Theta_{swu} = 0.00$, $\Theta_{swl} = 0.00$ in region IV). (c) $Re = 90$ ($\Theta_{swu} = 0.00$, $\Theta_{swl} = 0.00$ in region III).

Table 2. Liapunov spectrum

$Re = 220$	Region I	$d_m = 3$ [3±2, −5±2, −20±7]
		$d_m = 4$ [3±2, −3±2, −9±3, −28±7]
	Region III	$d_m = 3$ [21±5, 9±3, −13±8]
		$d_m = 4$ [20±5, 12±4, −4±5, −18±8]
$Re = 90$	Region III	$d_m = 3$ [11±3, 3±2, −11±7]
		$d_m = 4$ [10±3, 3±2, −4±3, −17±7]

i.e. when a pair of stable longitudinal rolls exist in the duct, the spanwise time-averaged Sherwood number distribution is not uniform. The distribution takes the minimum value at the middle of the bottom and increases towards the side walls where the large concentration gradient is caused by the downward secondary flow along the side walls. But the streamwise distribution as shown in Fig. 6(b) by mark ▽ becomes almost uniform except for the region that is less than about 20 mm (0.5 *De*) distant from the leading edge of the naphthalene plate. In contrast, for the case of unsteady flow in region III of Fig. 3(b), which gives rise to a time-averaged spanwise uniform temperature distribution, the spanwise Sherwood number distribution is fairly uniform as shown by mark ◇ in Fig. 6(a), and the streamwise distribution in this case is also almost flat except for the above-described region. This means that a chaotic flow with some mixing effect produces a spaciously uniform time-averaged Sherwood number distribution in the naphthalene surface. Such uniform distributions as shown in Figs. 6(a) and (b) are also obtained for all other side-wall temperature conditions in the same region III of Fig. 3(b) such as $\Theta_{swu} = 0.17$, $\Theta_{swl} = 0.54$. For $Re = 90$, however, the time-averaged Sherwood number distribution on the bottom wall has a non-flat distribution in the spanwise direction, as expected from the thermal feature of Fig. 4(b).

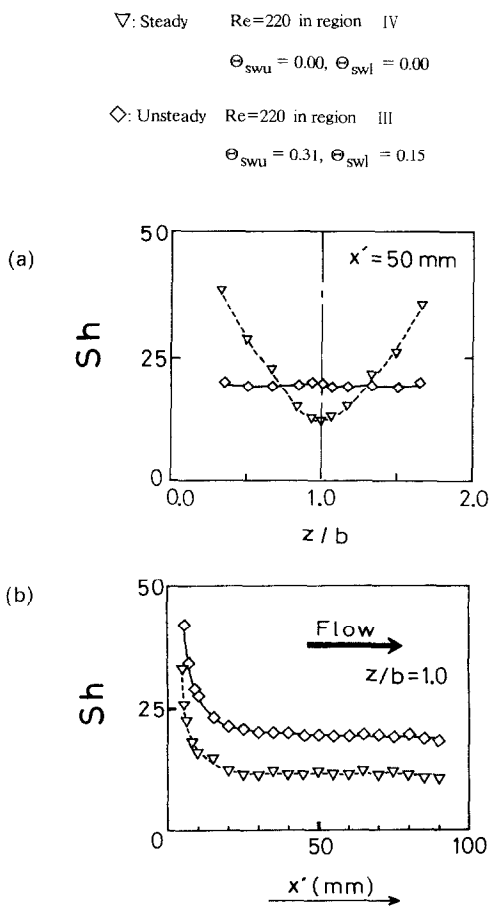

FIG. 6. Time-averaged Sherwood number distribution on the bottom wall for $Re = 220$. (a) Spanwise distribution. (b) Streamwise distribution.

Thus, we may expect to obtain the uniform growth of a thin semiconductor layer in a horizontal thermal CVD reactor, only by properly setting the side-wall temperature profile so as to make a chaotic flow which seems to have a favorable mixing effect.

4. CONCLUSION

We have performed an experimental research concerning the effects of the side-wall temperature profile to the flow in the fully-developed region of a horizontal rectangular duct of aspect ratio 2 heated from below, and revealed the condition on which the horizontally uniform time-averaged fluid temperature and mass transfer rate on the duct bottom wall are produced. The experiments were performed for Reynolds numbers ranging from zero to 500 and a Rayleigh number of about 3.4×10^5 and with various side-wall temperature profiles in between the top and the bottom wall temperature.

The conclusions obtained are as follows.

(1) By the flow visualization, the stable and unstable longitudinal rolls occur for Reynolds number ranging from 140 to 500; while only an unsteady flow is always found for Reynolds number below 140 but no specific vortices appeared.

(2) For Reynolds number 500, a pair of steady longitudinal rolls always exist in the duct. When the side wall temperature is high, the secondary flow is upward along the side walls. But when the side wall temperature is low, the longitudinal rolls rotate oppositely. At this Reynolds number, the fluid temperature is never uniform horizontally.

(3) For Reynolds number 220, three typical flow patterns depending on the temperature profile of the side walls appear, one is an unsteady flow with a time-averaged uniform temperature, the second is a flow

with a pair of longitudinal rolls and the other is a flow with similar rolls but with the opposite circulation. In the case of an unsteady flow, the temperature fluctuation intensity is about 3% and the power spectrum has many peak frequencies expressed as linear combinations of two basic frequencies. Furthermore, the time-averaged local mass transfer rate on the bottom wall becomes almost uniform in both the spanwise and the streamwise direction and this flow is favorable for thermal CVD reactors.

(4) For Reynolds number below 140, an unsteady flow is always found and no specific vortices are observed by the flow visualization. The time-averaged temperature on horizontal planes has a non-flat distribution and the temperature fluctuation intensity is about 5%. The power spectrum has many peak frequencies expressed as linear combinations of two basic frequencies.

(5) Unsteady flows for Reynolds number 220 and 140 were found to be chaotic by calculating a set of Liapunov exponents from the time series of fluid temperature.

Acknowledgement—The authors are grateful to Dr Y. Mori, Professor Emeritus of Tokyo Institute of Technology, for his valuable advices and many suggestions throughout this work.

REFERENCES

1. H. K. Moffat and K. F. Jensen, Complex flow phenomena in MOCVD reactors, *J. Crystal Growth* **77,** 108–119 (1986).
2. H. K. Moffat and K. F. Jensen, Three-dimensional flow effects in silicon CVD in horizontal reactors, *J. Electrochem. Soc.* **135,** 459–471 (1988).
3. J. Van de Ven, G. M. J. Rutten, M. J. Raaijmakers and L. J. Giling, Gas phase depletion and flow dynamics in horizontal MOCVD reactors, *J. Crystal Growth* **76,** 352–372 (1986).
4. T. A. Nyce, J. Ouazzani, A. Duraud-Daubin and F. Rosenberger, Mixed convection in a horizontal rectangular channel—experimental and numerical velocity distributions, *Int. J. Heat Mass Transfer* **35,** 1481–1493 (1992).
5. G. Evans and R. Greif, Unsteady three-dimensional mixed convection in a heated horizontal channel with applications to chemical vapor deposition, *Int. J. Heat Mass Transfer* **34,** 2039–2051 (1991).
6. K.-C. Chiu and F. Rosenberger, Mixed convection between horizontal plates—I. Entrance effects, *Int. J. Heat Mass Transfer* **30,** 1645–1654 (1987).
7. G. Evans and R. Greif, A study of traveling wave instabilities in a horizontal channel flow with applications to chemical vapor deposition, *Int. J. Heat Mass Transfer* **32,** 895–911 (1989).
8. I. Hosokawa, Numerical simulation of 3-D and no-slip bounded flows in a horizontal chemical vapor deposition duct. In *Computers and Computing in Heat Transfer Science and Engineering* (Edited by W. Nakayama and K.-T. Yang), pp. 43–58. CRC Press, Boca Raton (1993).
9. I. Hosokawa, Y. Tanaka and K. Yamamoto, Mixed convective flow with mass transfer in a horizontal rectangular duct heated from below simulated by the conditional Fourier spectral analysis, *Int. J. Heat Mass Transfer* **36,** 3029–3042 (1993).
10. H. Koizumi and I. Hosokawa, Controlling the generation of Bénard cells in combined convection of a horizontal rectangular duct heated from below (Experiment of mass transfer), *Trans. J.S.M.E.* (in Japanese) **B58,** 891–897 (1992).
11. H. Koizumi and I. Hosokawa, Generation and control of longitudinal rolls in combined convection in a horizontal rectangular duct heated from below (Mass transfer on the duct bottom wall), *Trans. J.S.M.E.* (in Japanese), submitted.
12. M. Sano and Y. Sawada, Measurement of the Liapunov spectrum from a chaotic time series, *Phys. Rev. Lett.* **55,** 1082–1085 (1985).
13. I. Shimada and T. Nagashima, A numerical approach to ergodic problem of dissipative dynamical system, *Prog. Theor. Phys.* **61,** 1605–1616 (1979).
14. T. Morishita and M. Nomura, Effect of free stream turbulence on local heat and mass transfer from circular cylinder in cross flow, *Report of Ship Research Institute* (in Japanese) **5,** 169–195 (1968).
15. M. W. Rubesin and M. Inouye, Forced convection, external flows. In *Handbook of Heat Transfer* (Edited by W. M. Rohsenow and J. P. Hartnett), Section 8. McGraw-Hill, New York (1973).
16. Y. Mori and H. Koizumi, A study of controlling generation of a Benard cell in the laminar combined convection in a horizontal rectangular duct heated from below, *Trans. J.S.M.E.* (in Japanese) **B55,** 820–827 (1989).
17. Y. Mori, Some optimizing examples in forced convective heat transfer, *ASME J. Heat Transfer* **112,** 268–273 (1990).
18. Y. Mori, I. Hosokawa and H. Koizumi, Control of the formation of Benard cells in a horizontal rectangular duct heated from below, *Wärme- und Stoffübertragung* **27,** 195–200 (1992).
19. H. Koizumi and I. Hosokawa, Generation and control of longitudinal rolls in combined convection in a horizontal rectangular duct heated from below (Fully developed turbulent region), *Trans. J.S.M.E.* (in Japanese) **B57,** 1051–1056 (1991); *Heat Transfer—Jap. Res.* **21,** 139–150 (1992).